# Integrating MACSPI and SILAC for Neuron Type-specific Proteomics in *Caenorhabditis elegans*


## Authors

Qiao Ran, Siyue Huang, Xiang David Li, and Chaogu Zheng

## Correspondence

cgzheng@hku.hk



## In Brief

Using the Methionine Analog-based Cell-Specific Proteomics and Interactomics (MACSPI) method, we conducted a comparative proteomic analysis of eight dopaminergic neurons (DA) and six touch receptor neurons (TRN) in *C. elegans*. This study showed the utility of MACSPI coupled with SILAC to profie the proteomes of specific types of neurons without physical isolation of the target cells, demonstrating the possibility of profiling scarce cell type-specific proteins from the lysate of complex tissues or the whole animal.


## Graphical Abstract

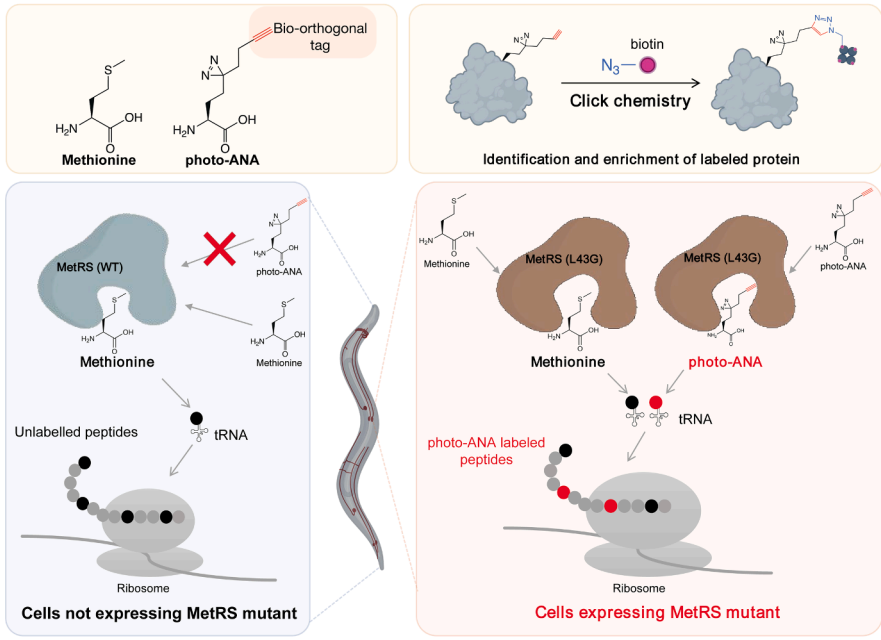


## Highlights

- Methionine analog photo-ANA labels the proteome of specific neurons.
- Click chemistry enables enrichment of neuron type-specific proteome from lysate.
- SILAC mediated quantitative proteomic profiling of two neuron types in *Caenorhabditis elegans.*
- Proteomic profiling of differentially expressed proteins between two neuron types.
- Weak correlation between protein and mRNA abundance in specific neurons.

**2026, Mol Cell Proteomics *25(4)*, 101545**

**https://doi.org/10.1016/j.mcpro.2026.101545**

# Integrating MACSPI and SILAC for Neuron Type-specific Proteomics in *Caenorhabditis elegans*

Qiao Ran[1], Siyue Huang[2], Xiang David Li[2], and Chaogu Zheng[1,*]

**Understanding neuronal differentiation and function requires precise proteomic characterization of distinct neuron types, yet existing methods face challenges in specificity and sensitivity. Here, we combine Methionine Analog-based Cell-Specific Proteomics and Interactomics (MACSPI) and SILAC to achieve neuron type-specific proteomic profiling in *Caenorhabditis elegans*. We demonstrate the utility of the methods by profiling and comparing the proteomes of two neuron types, namely the eight dopaminergic neurons (DA) and the six touch receptor neurons (TRNs). By expressing in these neurons an engineered methionyl-tRNA synthetase that can attach a methionine analog with a chemical handle to the synthesizing proteins, we chemically label the proteomes of specific neurons in complex tissues and isolate the labeled proteins from the whole-animal lysates through click chemistry and affinity purification. Thus, our approach does not require physical isolation of the neurons through cell sorting. Quantitative mass spectrometry studies through SILAC enable proteomic profiling and comparison of DA and TRNs and reveal distinct functional signatures between these two neuron types, with DA neurons showing enrichment in synaptic and metabolic pathways, while TRNs were characterized by cytoskeletal and signaling components. Moreover, we observed a weak correlation between protein abundance and mRNA levels, underscoring the importance of proteomic measurements. Our study establishes MACSPI-SILAC as a versatile platform for cell-type-specific proteomics in multicellular organisms, bridging a critical gap between transcriptomic and functional analyses. The proteomic datasets provide a resource for exploring the mechanisms of neuronal fate specification and cellular differentiation.**

Single-cell DNA and RNA sequencing technologies enable the characterization of biological features at the single-cell level, creating unprecedented spatial resolution in the analysis of complex tissues (1, 2). However, a fundamental limitation of genomic and transcriptomic profiling is that these indirect measures of cellular state cannot capture protein-level changes, thereby preventing the understanding of any post-transcriptional regulation in the cells (3, 4). Interestingly, a recent study noted that while the transcriptome is highly dynamic, the proteome provides complementary information of gene regulation shaped by protein synthesis, turnover, and post-translational modifications (PTMs), highlighting the need to analyze cellular states at the proteomic level (2, 5). Advancements in mass spectrometry (MS)-based proteomics allowed the profiling of the *Caenorhabditis elegans* proteome at the population (6), single-organism (7), and dissected tissue scales (8), utilizing standard proteomic workflows involving sample reduction, enzymatic digestion, and subsequent mass spectrometric characterization (9, 10). Through a chemical labeling approach using unnatural amino acids as probes, we and others have also demonstrated the possibility of profiling the proteomes of specific organs (such as the pharyngeal muscles, body wall muscles, and the nervous system) (11, 12). Prior to this study, robust proteomic profiling of defined neuron types in intact animals has rarely been accomplished.

Traditionally, cell-specific proteomics involves physically isolating the cell of interest from complex tissues through cell sorting. However, the cell sorting step may lead to the loss of cellular compartments (*e.g.*, neurons may lose the axon and dendrites during the sorting), potential bias for certain cell sizes, contamination of other tissues (due to incomplete tissue dissociation), and stress-related artifacts (due to the prolonged processing time) (13–15). To overcome the abovementioned limitations, tissue-specific *in situ* protein labeling strategies were developed. These chemical biology approaches rely on the labelling of cell-specific proteomes with an unnatural amino acid that contains a bio-orthogonal handle, which is then used to extract the labeled proteins from the whole-animal or whole-tissue lysates, bypassing the need for cellular isolation. Based on this strategy, we previously established a method named Methionine Analog-based Cell-Specific Proteomics and Interactomics (MACSPI) (12), which tags proteins expressed in specific tissues with a

From the [1]School of Biological Sciences, Faculty of Science, and [2]Department of Chemistry, The University of Hong Kong, Hong Kong, China
*For correspondence: Chaogu Zheng, cgzheng@hku.hk.





https://doi.org/10.1016/j.mcpro.2026.101545

methionine analog photo-ANA that contains an alkyne group. The photo-ANA probe also contains a diazirine group for photo-crosslinking, although this functionality is not used in this study. The tissue-selective proteomic labeling is achieved by expressing an engineered methionyl-tRNA synthetase (MetRS) mutant capable of attaching photo-ANA in place of methionine to $tRNA^{Met}$ in selective tissues. Since wild-type MetRS cannot charge $tRNA^{Met}$ with photo-ANA, only the proteins synthesized in the tissues expressing mutant MetRS are labelled by photo-ANA. Following the *in vivo* labeling, photo-ANA-tagged proteins bearing an alkyne group can be extracted using copper-catalyzed azide-alkyne cycloaddition (click chemistry), enabling their selective enrichment from total lysates for downstream proteomic analysis (graphic abstract) (12).

With regards to quantitative MS, the existing methods fall into two major categories: one that involves isobaric tagging (*e.g.*, TMT, iTRAQ) and one that uses stable isotopes (e.g., mTRAQ, SILAC, and dimethyl labeling) (2). Although isobaric tagging enables signal amplification through precursor intensity summation in multiplexed samples and is conveniently carried out after protein extraction and before the MS analysis, the methods fail to account for factors in sample preparation. In contrast, SILAC shows advantages in quantitative accuracy and reproducibility over isobaric labeling approaches. Because SILAC is based on the direct addition of stable isotope amino acids into the culturing medium, the differentially treated samples can be combined in the form of whole animal/tissue lysate at the very first step of the experimental workflow, and the combined samples can then be processed together in the same tube to minimize batch effects, experimental errors, or other potential bias. Although SILAC offers lower multiplexity than the isobaric labeling method (such as TMT) or label-free quantification methods, it is more accurate and highly reproducible when only two or a few different conditions/treatments are examined in one experiment. In this study, we combined MACSPI with SILAC to enable cell-specific proteome profiling and comparative proteomic analysis across distinct neuron types (12).

As a proof of concept, we focused on two neuron types in *C. elegans*, namely the dopaminergic neurons (DA) and the touch receptor neurons (TRNs). The cell fate specification mechanisms for these neurons have been previously studied (16–19), and their gene expression profiles were analyzed at the transcriptome level (20–23). However, the proteomes of these well-characterized neuron types in *C. elegans* remain poorly understood. The eight dopaminergic neurons (including four pairs of laterally symmetric neurons, namely ADEL/R, CEPDL/R, CEPVL/R, and PDEL/R) are ciliated mechanosensory neurons that detect the texture of the environment when crawling through bacteria and communicate with the motor circuit to reduce locomotion rate (24–27). On the other hand, the six touch receptor neurons (including the ALML/R, PLML/R, AVM, and PVM) are glutamatergic mechanosensory neurons that are non-ciliated, detect gentle body touch, and stimulate the motor program to elicit the escape response (28, 29). Thus, understanding the difference in the protein expression profiles of DA and TRN neurons could help identify key mechanisms that enable the differentiation of their specific morphologies and functions. Furthermore, the DA neurons in *C. elegans* have been used as a Parkinson's disease model to study α-synuclein aggregation-induced neurodegeneration (30–32), while the TRNs are used as a prime model for axonal regeneration in invertebrates (33, 34). Thus, characterizing the proteins expressed in these neurons may provide insights into the mechanisms of neuronal degeneration and regeneration.

In this study, using MACSPI coupled with SILAC, we profiled the proteomes of *C. elegans* DA and TRN neurons at the fourth larval stage. We identified 774 and 760 proteins expressed in the DA and TRN neurons, respectively. Among the DA proteome, there are several known functionally significant proteins, including RAB-3 (synaptic vesicle protein (35)), EGL-30 (a Gq protein that modulates synaptic transmission (36, 37)), and GAS-1 (an NADH dehydrogenase essential for mitochondria (38)); and among the TRN proteome are MEC-7 (β-tubulin (39)), UNC-44 (ankyrin regulating axonal growth (40)), and PAT-3 (β-integrin regulating touch sensation (41)). We also identified DA and TRN proteins whose expression patterns were previously uncharacterized. For many of these unstudied genes, we created GFP reporters to validate that they are indeed expressed in the DA or TRN neurons. Furthermore, by labeling DA and TRN proteomes with different isotopes, we designed a SILAC experiment to directly compare their proteomes and identified differentially expressed proteins through quantification. Such analysis led us to uncover neuron-type-specific proteins. In general, the abundance levels of proteins are weakly correlated with their mRNA levels in both neuron types, suggesting potential posttranscriptional regulation. In summary, we demonstrated the possibility of using MACSPI coupled with SILAC to profile the proteome of a few neurons in an intact animal (*C. elegans* hermaphrodite) with 959 somatic cells (including 302 neurons) and ~400 germ cells. This method can be broadly used to uncover posttranscriptional regulatory mechanisms in specific types of cells.

## EXPERIMENTAL PROCEDURES

### *Constructs, Transgenes, and the* C. elegans *Strains*

*C. elegans* strains were maintained at 20 °C using previously described methods (42). To create *Ce*MetRS expression constructs, we cloned the *mars-1* coding sequence with a L43G mutation and a C-terminal 2xFLAG tag (12) into a pDEST (Invitrogen) vector downstream of either a 0.7 kb *dat-1* promoter (for DA neurons) or a 1.9 kb *mec-17* promoter (for TRNs) and upstream of an *unc-54* 3′-untranslated region. Cloning was carried out using Gibson Assembly (NEB). The cloned plasmids were then injected into *unc-119(ed3)* mutants with *Cbr-unc-119(+)* as a co-injection marker. Gamma-irradiation was

used to integrate the extrachromosomal arrays, and the integrated transgene was outcrossed 6 times to remove background mutations. Transcriptional reporters were generated by cloning candidate gene promoters and inserting them to the upstream of a GFP sequence. Plasmids were co-injected together with a neuron type-specific RFP marker (*dat-1p::RFP* for DA neurons or *mec-17p::TagRFP* for TRNs) and a *Cbr-unc-119(+)* selection marker into *unc-119(ed3)* animals to create transgenic lines. Reporter expression was then validated by the colocalization of GFP with the corresponding RFP neuronal marker. All strains used in this paper are listed in the appendix (Supplemental Table S1).

### *Experimental Design and Statistical Rationale*

This SILAC-MS-based proteomic study was designed to balance statistical rigor with the practical constraints of conducting the chemoproteomic labeling (*i.e.*, the requirement of a significant amount of the photo-ANA probe). For each profiling experiment, we prepared two biological replicates, each representing a separately cultured and processed *C. elegans* population. The two replicates were carried out independently throughout the MACSPI-SILAC workflow followed by LC-MS/MS. To mitigate the concern of a low number of replicates, we called the hits by requiring the proteins to have standout H/L ratio [$Log_2$(H/L) > 0.5] in both replicates. This approach is then supplemented by a statistical analysis using a two-tailed, two-sample Student's *t* test with two degrees of freedom. The null hypothesis was defined as the $Log_2$(H/L) being equal to zero (*i.e.*, no change). For each protein, the test was performed by comparing the array of its two replicates of $Log_2$(H/L) measurements against an array of two zeros representing the null hypothesis. The resulting *p*-values were corrected using the Benjamini-Hochberg procedure with 5% false discovery rate (FDR). A protein was considered significantly enriched if the average $Log_2$(H/L) > 0.5 and an FDR-adjusted *p*-value <0.05. This statistical analysis allowed us to identify additional standout proteins.

### *SILAC Profiling of Neuron Type-Specific Proteomics in* C. elegans

For the SILAC experiment, we used a previously engineered *Escherichia coli* strain CGZ1760, which is a *ΔargA/ΔlysA/ΔmetB* triple knockout expressing *Ec*MetRS L13 G and dsRNAs against the *C. elegans oatr-1* gene from the T7 promoter (12). M9 minimal medium containing 6 g/L $Na_2HPO_4$, 3.2 g/L $KH_2PO_4$, 0.5 g/L NaCl, 1 g/L $NH_4Cl$, and 40 mg/L of 17 amino acids (all essential and non-essential amino acids except arginine, lysine, and methionine) was first autoclaved at 121 °C for 20 min for sterilization, and then 0.2% (wt/vol) glucose (filtered by 0.2 μm membrane, Cytiva) and 2 mM $MgSO_4$ (autoclaved separately) were added to the medium, which became a base for *E. coli* culturing. 200 ml of *E. coli* strain CGZ1760 was first cultured in "heavy" medium (M9 minimal medium supplemented by 40 mg/L methionine, 40 mg/L arginine-$^{13}C_6{}^{15}N_4{}^{1}H_{14}{}^{16}O_2$, and 40 mg/L lysine-$^{13}C_6{}^{15}N_2{}^{1}H_{14}{}^{16}O_2$), concentrated, and fed to *C. elegans* strains (CGZ715 or CGZ2302) expressing the *Ce*MetRS L43G mutant from the DA- or TRN-specific promoter, respectively, in a small scale for 3~4 generations to replace most of the "light" arginine and lysine in *C. elegans*. For the heavy labeling with photo-ANA, we conducted two rounds of labeling. For the first round, the above animals were first transferred to the M9 minimal plates supplemented by 2 mM photo-ANA in the agar and seeded with concentrated "heavy" *E. coli* labeled in 800 ml "heavy" medium (M9 minimal medium with 4 mM photo-ANA, 40 mg/L arginine-$^{13}C_6{}^{15}N_4{}^{1}H_{14}{}^{16}O_2$, and 40 mg/L lysine-$^{13}C_6{}^{15}N_2{}^{1}H_{14}{}^{16}O_2$). The animals were grown to the adult stage and then bleached to extract the eggs, which were then synchronized at the L1 stage. For the second round of labeling, the above L1 animals were fed with concentrated "heavy" *E. coli* that were labeled in 1000 ml "heavy" medium (M9 minimal medium with 4 mM photo-ANA, 40 mg/L arginine-$^{13}C_6{}^{15}N_4{}^{1}H_{14}{}^{16}O_2$, and 40 mg/L lysine-$^{13}C_6{}^{15}N_2{}^{1}H_{14}{}^{16}O_2$) and seeded on M9 minimal medium plates containing 2 mM photo-ANA. The animals were grown for 48 h to reach the L4 stage before being harvested. This protocol was optimized to maximize both heavy isotope and photo-ANA labeling.

For the "light" batch animals without photo-ANA labeling, the same transgenic animals were similarly cultured on M9 minimal medium plates seeded with "light" CGZ1760 *E. coli* grown in "light" medium (M9 minimal medium with 40 mg/L methionine, 40 mg/L arginine-$^{12}C_6{}^{14}N_4{}^{1}H_{14}{}^{16}O_2$, and 40 mg/L lysine-$^{12}C_6{}^{14}N_2{}^{1}H_{14}{}^{16}O_2$) for one generation. The animals were then bleached and synchronized to the L1 stage, and the L1 animals were then fed with concentrated *E. coli* cultured in 1000 ml of "light" medium (M9 minimal medium with 40 mg/L methionine, 40 mg/L arginine-$^{12}C_6{}^{14}N_4{}^{1}H_{14}{}^{16}O_2$, and 40 mg/L lysine-$^{12}C_6{}^{14}N_2{}^{1}H_{14}{}^{16}O_2$) on M9 minimal plates without photo-ANA supplementation. The light animals were also grown for 48 h to the late L4 stage.

Both "heavy" (and photo-ANA-labeled) and "light" worms were washed off the plates and incubated in M9 buffer for 1h to allow the excretion of gut bacteria. This step is important for removing the contamination from the labeled *E. coli*. The animals were then lysed in SDS lysis buffer (1% SDS, 50 mM HEPES, 150 mM NaCl, 2 mM $MgCl_2$, 0.1% tween-20, 20% glycerol, 0.5 mM phenylmethylsulfonyl fluoride (PMSF), and 1 × protease inhibitor cocktail (cat#4693159001, Sigma Aldrich)) and homogenized by the Mini-BeadBeater 16 (Biospec Products) using glass beads (0.5 mm, Biospec Products). BCA Protein Assay (Thermo Fisher Scientific) was used to determine the protein concentrations. Lysates containing 30 mg of proteins of both "heavy" and "light" samples were mixed in a 1:1 ratio as the starting material. The lysate was first incubated with streptavidin beads in a pre-clean-up step to remove endogenous biotinylated proteins, which helps enhance the detection sensitivity for the relatively small number of proteins expressed in DA and TRN neurons. Click chemistry was then performed by reacting the lysate with 200 μM biotin-conjugated azide in the presence of 2 mM tris-(2-carboxyethyl)phosphine, 200 μM tris(-benzyltriazolylmethyl)amine, and 2 mM $CuSO_4$ at 25 °C for 90 min. Note that we increased the concentration of the azide and the catalyst compared to previous protocols to increase reaction efficiency (12, 43). Ice-cold acetone was then added to precipitate the proteins, which were subsequently dissolved in PBS buffer with 20 mM ethylenediaminetetraacetic acid, 4% SDS, and 10% glycerol at 85 °C. The protein samples were diluted with PBS to a final concentration of SDS lower than 0.5% and pulled down by incubating with 30 μl of streptavidin beads (cat#20359, Thermo Fisher) at room temperature for 3h. Streptavidin beads were then resuspended with 30 μl of loading buffer (LT101, EpiZyme), heated to 90 °C for 8 min, and alkylated with 130 mM iodoacetamide in the dark for 30 min.

### *SILAC-Based Quantification of Differentially Expressed Proteins Between DA and TRN Neurons*

*C. elegans* strain CGZ715 expressing *Ce*MetRS L43G mutants under the DA-specific promoter was grown in medium containing "heavy" isotopes (arginine-$^{13}C_6{}^{15}N_4{}^{1}H_{14}{}^{16}O_2$, lysine-$^{13}C_6{}^{15}N_2{}^{1}H_{14}{}^{16}O_2$) and photo-ANA, while the strain CGZ2302 expressing *Ce*MetRS L43G mutants under the TRN-specific promoter was cultured in medium containing "light" isotopes (arginine-$^{12}C_6{}^{14}N_4{}^{1}H_{14}{}^{16}O_2$, lysine-$^{12}C_6{}^{14}N_2{}^{1}H_{14}{}^{16}O_2$) and photo-ANA. Both strains were labeled for at least two generations. Animals were grown to the L4 stage, lysed, and subjected to click chemistry, streptavidin enrichment, and protein extraction, like the procedures described above.

### *Trypsin Digestion and Peptide Purification*

The enriched proteins from the above steps were separated by NuPAGE 4 to 12%, Bis-Tris gel (NP0321BOX, Thermo Fisher) and subjected to in-gel digestion using Pierce Trypsin Protease (cat#90057, Thermo Fisher Scientific) overnight at 37 °C. The resulting peptides were extracted with 150 μl of buffer containing 1.7% formic acid and 67% ACN twice from the gel, concentrated to nearly dry by vacuum concentrator (SpeedVac, 55 °C), and resuspended in 200 μl of 0.1% trifluoroacetic acid. We then prepared StageTips by stuffing a three-layer membrane (66883-U, Sigma Aldrich) into the head of 250 μl tips (cat#30389194, RAININ), and washed the tips with 80 μl of the following washing buffers in the order: a) pure methanol, b) 0.1% trifluoroacetic acid, c) 0.1% trifluoroacetic acid; 70% acetonitrile, d) 0.1% trifluoroacetic acid, and e) 0.1% trifluoroacetic acid. The dissolved peptides were transferred to the prepared StageTips, trapped by the membrane upon 1500 g centrifugation, subsequently washed with 0.5% acetic acid, and eluted twice with 50 μl of 40% acetonitrile, 0.5% acetic acid, and then 50 μl of 60% acetonitrile, 0.5% acetic acid. The elutes were subsequently dried under a vacuum concentrator to remove the solvent. The peptide powders were then dissolved in 20 μl of 0.1% formic acid for subsequent LC-MS/MS analysis.

### *LC-MS/MS Analysis*

The samples were analyzed using a Q Exactive Plus mass spectrometer (Thermo Scientific) coupled with an Ultimate 3000 RSLCnano system (Dionex). Chromatographic separation was achieved using a PepMap 100 C18 trapping column (5 μm, 300 μm × 5 mm) and a PepMap RSLC C18 analytical column (2 μm, 75 μm × 25 cm). Peptides were eluted with a 160-min linear gradient of 0 to 80% acetonitrile (0.1% formic acid) at a flow rate of 250 nl/min, with electrospray ionization applied *via* a PEEK junction (600–1800 V). MS data were acquired in data-dependent acquisition (DDA) mode and processed using Xcalibur 4.7. Full-scan MS spectra (375–1800 m/z) were collected in the Orbitrap at a resolution of 120,000, followed by HCD-MS/MS of the top 20 most intense ions (isolation window: ±1.6 m/z, resolution: 15,000). Automatic gain control (AGC) targets were configured at $4 \times 10^5$ ions for full MS scans and $5 \times 10^4$ ions for MS/MS scans, with maximum injection times set to auto and 27 ms, respectively. HCD-MS2 fragmentation was performed using a 28% normalized collision energy, with exclusion of singly charged, >8+ charged, and unassigned charge state ions from MS2 analysis.

### *Proteomic Data Analysis*

All LC-MS/MS raw data were processed using Proteome Discoverer (v. 3.0) against a UniProt *C. elegans* database containing 27,442 genes (October 24th, 2024 version). Quantification was performed using the SILAC 2plex method (Arg10, Lys8), with protein ratio calculations based on protein abundance. The confidence threshold for the target false discovery rate (FDR) was set to 0.01 for strict criteria and 0.05 for relaxed criteria. The precursor mass tolerance was configured at 20 ppm, and the fragment mass tolerance was set at 0.5 Da with up to two missed cleavages. Oxidation (+15.995 Da) and acetylation (+42.011 Da) at the protein N-terminus were designated as dynamic modifications, while carbamidomethylation (+57.021 Da) was assigned as a static modification. The minimum trace length was configured to 5, and a peptide length was restricted to a range of 6 to 144 amino acids. Peptide spectrum matches were filtered based on a mass accuracy within 10 ppm. All remaining parameters were maintained at their default configurations as specified by the software. For the profiling of DA- and TRN-specific proteome, we used the "Abundance Ratios ($Log_2$): (Heavy)/(Light)" results generated by Proteome Discoverer, while for the differential gene expression comparing DA and TRN proteomes, we used the "Abundance (Normalized)" results in the output file to calculate the $Log_2$(H/L) values.

### *GO and KEGG Analysis*

Differentially expressed genes (DEGs) were functionally annotated using Gene Ontology (GO) terms across three categories (biological process, molecular function, and cellular component) via DAVID, with statistical significance assessed by hypergeometric tests (adjusted $p < 0.05$) (44). For pathway analysis, DEGs were mapped to the KEGG database, and overrepresentation analysis was performed to identify significantly enriched pathways based on gene counts (44). For all pathway enrichment analyses, the background was defined as the complete *C. elegans* proteome.

### In Situ *Click-Chemistry and In-Gel Fluorescence*

We used a previous protocol for *in situ* click chemistry (12). Briefly, photo-ANA-labeled *C. elegans* strains were fixed with ice-cold fixing solution (80 mM KCl, 20 mM NaCl, 10 mM EGTA, 15 mM PIPES, pH 7.4, 5 mM spermidinetrihydrochloride, 25% methanol, and 2% formaldehyde), and we used freeze-thaw cycles to crack the worm cuticle. The samples were treated with Tris-Triton buffer (100 mM Tris HCl, pH 7.4; 1% Triton X-100; 1 mM EDTA), 1% 2-mercaptoethanol in borate buffer (25 mM $H_3BO_3$, 0.01% Triton X-100), 10 mM DTT in borate buffer, 0.3% hydrogen peroxide in borate buffer, and 0.5% Triton X-100 in PBS consecutively with washing with borate buffer in between. The treated worm samples were then reacted with 5 μM rhodamine-azide by "click" chemistry (400 μM TCEP, 200 μM TBTA, and 200 μM $CuSO_4$) for 2 h in the dark at room temperature, washed with PBDTT buffer (1% DMSO, 0.1% Tween-20, 0.5 mM EDTA, and 0.5% Triton X-100 in PBS), and then treated with blocking buffer (5% BSA, 0.5% Triton X-100, 5 mM $NaN_3$, and 1 mM EDTA in PBS). Anti-FLAG mouse monoclonal antibody (F1804, Sigma Aldrich) was then added to the sample for incubation on a rotator at 4 °C overnight. Worms were then washed in PBST-B buffer (0.1% BSA, 0.5% Triton X-100, 5 mM $NaN_3$, and 1 mM EDTA in PBS), followed by incubation with secondary antibody anti-mouse Alexa Fluor 488 (A32723, Thermo Fisher Scientific) in blocking buffer at room temperature for 2 h and washed with PBST-B buffer before being mounted on a microscopic slide.

In-gel fluorescence was conducted using a previous protocol (12). Photo-ANA-labeled *E. coli* or *C. elegans* were lysed by SDS lysis buffer and homogenized by sonication. Lysates were centrifuged at 15,000*g* at 4 °C for 10 min. The supernatant was collected. For the click chemistry reaction, 200 μM rhodamine-azide was added to lysates, followed by 2 mM tris(2-carboxyethyl) phosphine hydrochloride and 200 μM tris[(1-benzyl-1H-1,2,3-triazol-4-yl) methyl] amine, and 2 mM $CuSO_4$. Lysates were incubated for 1 h in the dark at room temperature. Proteins were precipitated by four volumes of ice-cold acetone at −20 °C and then collected by centrifugation at 16,000*g* at 4 °C for 10 min. Protein pellets were washed with methanol and dried in air. Proteins were resuspended in LDS sample loading buffer (Thermo Fisher Scientific) with 50 mM DTT, heated at 85 °C for 8 min, and separated by SDS-PAGE. The photo-ANA-labeled proteins were visualized by scanning the gel on a Typhoon 9500 molecular imager (GE Healthcare) with excitation at 532 nm and emission at 580 nm. Protein gels were stained with Coomassie Brilliant Blue (BioRad) to confirm equal loading.

### *Fluorescence Imaging*

Fluorescence imaging was carried out using a Leica DMi8 epi-fluorescent microscope equipped with a K5 sCMOS Camera and

deconvolution by Thunder software. To examine the GFP reporters, young adults were mounted on 3% agarose pads containing the anesthetics 2,3-Butanedione monoxime (BDM). Measurements of fluorescence intensity were made by the LAS X software. In general, at least 20 worms were examined for each strain. Fixed worms were mounted in a drop of M9 on agarose pads without BDM.

## RESULTS

### *Photo-ANA Labeling of Proteins Synthesized in Specific Types of Neurons*

To adopt SILAC in *C. elegans*, we used an auxotrophic *E. coli* strain CGZ1760 (*ΔmetB/ΔlysA/ΔargA*) that can be metabolically labeled with photo-ANA (Fig. 1*A*) and can deliver dsRNA against the *C. elegans oatr-1* gene (which codes for an ornithine aminotransferase that can promote arginine synthesis from other amino acids) as the food source for *C. elegans* (12). To use MACSPI to profile the proteomes of DA and TRN neurons, we created transgenic animals expressing the *C. elegans* methionyl tRNA synthetase (*mars-1* or *Ce*MetRS) L43G mutants specifically in the DA and TRN neurons. This *Ce*MetRS mutant was previously shown to be able to charge methionyl $tRNA^{Met}$ with photo-ANA, which could not be attached to tRNA by wild-type *Ce*MetRS (12). After labeling the *E. coli* and the transgenic animals with photo-ANA, we collected their lysate and analyzed them via *in vitro* click chemistry with rhodamine-azide and in-gel fluorescence scanning (Fig. 1, *A* and *B*). The results confirmed successful labeling of both bacterial and *C. elegans* proteins with the probe. To validate that only proteins expressed in specific *C. elegans* neurons were labeled by photo-ANA, we conducted *in situ* click chemistry to conjugate rhodamine-azide with the alkyne group on photo-ANA in the intact worms. The results showed specific labeling of only the DA or TRN neurons that expressed the FLAG-tagged *Ce*MetRS (L43G) in the entire animal, which confirmed the neuron type-specific proteome labeling (Fig. 1*C*).

### *Profiling the Proteome of Dopaminergic Neurons in* C. elegans

We previously demonstrated the possibility of profiling the proteomes of the body wall muscles and the entire nervous system using the MACSPI method (12). However, compared to the proteomic profiling of 95 body wall muscle cells and 302 neurons in the *C. elegans* hermaphrodites, profiling the proteomes of eight DA neurons or six TRNs was technically much more challenging. To increase the detection sensitivity of the MACSPI method, we optimized the workflow by (1) growing the transgenic animals in "heavy" medium for several generations to achieve more complete metabolic replacement of light arginine and lysine, ensuring a high signal-to-noise ratio for SILAC quantification, (2) labeling the animals with photo-ANA for two generations to increase labelling efficiency toward saturation, (3) increasing the concentration of photo-ANA and adding them into the culturing medium for both bacteria and *C. elegans* to enhance the bioavailability, (4) adding a step of pre-cleanup with streptavidin beads to remove endogenous biotinylated proteins, thereby reducing non-specific background and facilitating the effective enrichment of low-abundance neuronal proteins, and (5) increasing the reagents' concentration in the click-chemistry reaction to maximize conjugation efficiency (see Experimental Procedures for details).

For the SILAC setup, we first fed the transgenic animals with either "heavy" bacteria labeled with photo-ANA or "light" bacteria grown with methionine (Fig. 2*A*). The worms were then lysed, and the lysates from the "heavy" and "light" conditions were combined in a 1:1 ratio and subjected to conjugation with biotin-azide and protein extraction using the streptavidin beads. The extracted proteins were then processed for trypsin digestion, mass spectrometry analysis, and proteomic profiling (Fig. 2*A*). Proteins with high heavy-to-light (H/L) ratios were qualified as proteins from the specific neurons labeled with photo-ANA. Proteins that were only detected in the heavy sample but not the light sample (thus they do not have H/L ratios) could still be expressed in the neurons of interest but were not included in the initial analysis.

For the DA proteome, by filtering for proteins with $Log_2$(H/L) values greater than 0.5 in both replicates, we identified 396 proteins, 82% of which have mRNA expression in the DA neurons according to published single-cell transcriptomic data (Fig. 2*B* and Dataset S1) (45). The enrichment fold is 2.35 ($p$ = 1.35e-83 in a hypergeometric test), supporting that these proteins are expressed in DA neurons. We chose the threshold of $Log_2$(H/L) = 0.5 as the cutoff for calling hits because a higher threshold significantly reduced the number of proteins that can be identified without improving the enrichment for genes with mRNA expression in DA neurons. If we used the criteria that the average $Log_2$(H/L) of the replicates was greater than 0.5 and the adjusted $p$ value was smaller than 0.05 [equivalent to $-Log_{10}(p\text{-adj}) > 1.3$], we could identify 171 proteins, 89% of which have mRNA expression in the DA neurons with an enrichment fold of 2.55 ($p$ = 6.03e-81 in a hypergeometric test) (Fig. 2*C* and Dataset S1). The above 396 and 171 proteins identified using the two filtering methods largely overlap, and we combined them to generate a set of 400 proteins for the final DA proteome. It is worth noting that this number is likely an underestimate, since SILAC is a quite stringent method for proteomic profiling. In fact, we identified a total of 1790 proteins from the enriched samples, and 1445 of them have mRNA expression in the DA neurons (enrichment fold = 2.32; $p$ = 2.45e-282). We suspect that many of the proteins with $Log_2$(H/L) < 0.5 may still be expressed in DAs; because the "heavy" labeling is likely not 100%, some proteins may still contain significant amount of "light" arginine and lysine even if they are from the "heavy" sample and are labeled by photo-ANA (Supplemental Fig. S1*A*).

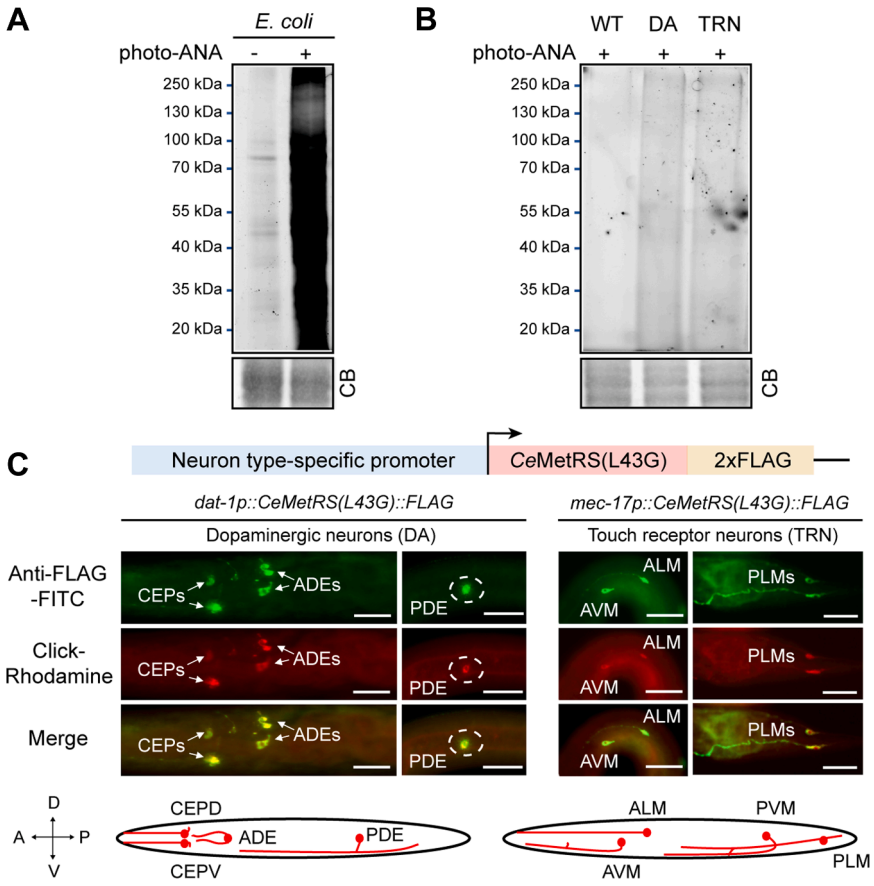


FIG. 1. **Photo-ANA incorporation into proteins in engineered *E. coli* and *C. elegans*.** *A*, in-gel fluorescence (*top*) and Coomassie blue staining (CB, *bottom*) of lysates from *E. coli* grown with or without 2 mM photo-ANA. Fluorescence confirms specific incorporation. *B*, in-gel fluorescence of *C. elegans* lysates shows photo-ANA incorporation in animals expressing *Ce*MetRS(L43G) in DA neurons and TRNs, but not in wild-type animals. *C*, co-localization of anti-FLAG staining (*green*, indicating *Ce*MetRS(L43G)::2×FLAG expression) and rhodamine signal from *in situ* click chemistry (*red*) confirms neuron type-specific photo-ANA labeling. Scale bar: 20 μm. A cartoon shows the location and morphology of DA neurons and TRNs in the animal. There are eight DA neurons (CEPDL/R, CEPVL/R, ADEL/R, PDEL/R) and six TRNs (ALML/R, AVM, PVM, PLML/R). Only one neuron of the bilaterally symmetric pairs is shown in the cartoon for simplicity.

Among the 400 genes identified in the DA proteome, many of them were known to be expressed in the DA neurons from previous studies, such as *goa-1* (encoding a Gα protein), *egl-30* (encoding another Gα protein), *sca-1* (encoding the Sarco-Endoplasmic Reticulum $Ca^{2+}$ ATPase), and *akt-1* (encoding AKT serine/threonine kinase) (46–49). Many proteins (*e.g.*, *cdd-2*, *F17A9.4*, *Y54F10AR.1*, and *F52E4.5*) showed significantly higher mRNA levels in DA neurons than their average mRNA levels across all neurons or in other tissues (such as muscles, intestine, and epidermis) according to the single-cell transcriptomic data, suggesting that they may be enriched in DA neurons (Fig. 2*D*). To further confirm the expression of the identified proteins in DA neurons, we selected a few candidate genes whose expressions were not studied using transcriptional reporters before and made GFP reporters. We confirmed that the expression of these genes, including *cest-32*, *F17A9.4*, and *F52E4.5*, in the DA neurons, indicating the utility of our proteomic profiling in identifying novel proteins in specific neurons (Fig. 2*E*). Additionally, proteins such as C32D5.8 do not stand out from the above criteria but still show GFP expression in ADE and PDE based on a transcriptional reporter (Supplemental Fig. S1*B*).

Gene ontology (GO) analysis identified functional enrichment of the DA proteins in GO terms related to intracellular protein transport, mitochondria structure and function, and energy metabolism, while Kyoto Encyclopedia of Genes and Genomes (KEGG) pathway analysis showed enrichment in pathways related to the ribosome, carbon metabolism, biosynthesis of amino acids, purine metabolism, and the proteasome (Fig. 2*F* and Supplemental Fig. S2 and Supplemental Dataset S2). Functional annotation of these proteins also led to the identification of many proteins involved in synaptic transmission (*e.g.*, the synaptic vesicle protein RAB-3), protein binding (*e.g.*, ITSN-1 involved in regulation of synaptic vesicle endocytosis), synaptic vesicle trafficking (*e.g.*, the dynein complex regulator NUD-1 involved

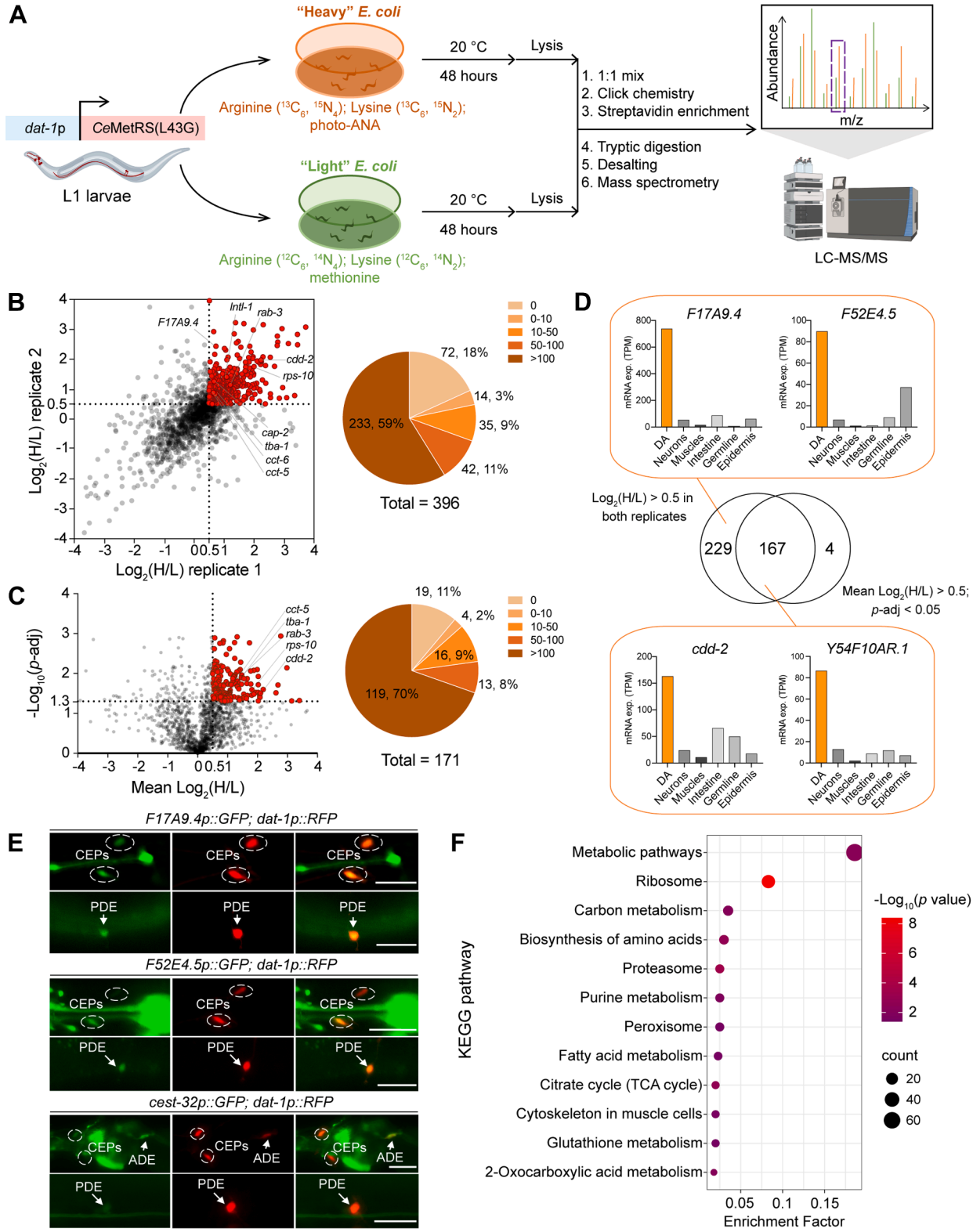


FIG. 2. **MACSPI-SILAC enables the profiling of the proteome in dopaminergic neurons.** *A*, a workflow of the SILAC-based labeling and profiling of proteins from DA neurons. *B*, reproducibility of proteomic quantification. Scatter plot of protein $Log_2$(H/L) ratios from two independent experiments (Pearson's correlation coefficient $r = 0.67$). Proteins enriched in both replicates [$Log_2$(H/L) > 0.5] are highlighted in *red*. The pie chart (*right*) shows the mRNA expression distribution of these highlighted proteins in DA neurons based on transcriptomic data. The full list can be found in Supplemental Dataset S1. *C*, statistical significance of protein enrichment. Volcano plot showing the relationship between

in organelle localization), and microtubule (*e.g.*, T-complex subunit CCT family proteins and TBA-1) (35, 50–53). The abovementioned results serve as a proof of concept for the possibility of profiling the proteome of a few neurons (belonging to a specific neuron type) from the lysate of an intact animal using the MACSPI-SILAC approach.

### *Profiling the Proteome of Touch Receptor Neurons in* C. elegans

To test the versatility of our approach across different neuron types, we conducted similar experiments to profile the proteome of six touch receptor neurons in transgenic *C. elegans* expressing *Ce*MetRS L43G mutants from the TRN-specific *mec-17* promoter (Fig. 3*A*). We identified 207 proteins with $Log_2$(H/L) above 0.5 in both replicates, and 76% of them have mRNA expression in the TRNs (enrichment fold = 2.19, $p$ = 7.36e-34 in hypergeometric test; Fig. 3*B* and Supplemental Dataset S3). We also identified 88 proteins with the average $Log_2$(H/L) above 0.5 and $p$-adj value < 0.05, 77% of which show mRNA expression in the TRNs (enrichment fold = 2.19, $p$ = 1.11e-14 in hypergeometric test; Fig. 3*C* and Supplemental Dataset S3). As expected, the two lists are highly overlapped; combining them, we obtained 210 proteins for the TRN proteome (Fig. 3*D*). Like the DA neuron case, there would probably be more proteins expressed in TRNs in our dataset if the criteria were relaxed (Supplemental Fig. S3*B*). We identified a total of 953 proteins from the mass spectrometry; 77% of all these proteins have mRNA expression in TRNs (enrichment fold = 2.19, $p$ = 3.22e-155 in hypergeometric test).

Among the proteins in the TRN proteome, many proteins were known to be expressed in TRNs from previous studies, such as MEC-7 (a TRN-specific β-tubulin), TBB-2 (another β-tubulin), VHA-2 (a vacuolar $H^+$-ATPase), VHA-12 (another V-ATPase), and UNC-44 (an ankyrin) (54–57). Several proteins showed enriched expression in TRNs, such as MCA-3 (calcium ATPase, whose loss leads to a reduction in touch sensitivity) and PAT-3 (β-integrin, whose binding activity enables sensitivity to anterior touch) (41, 58). We also created transcriptional reporters for several proteins that were not studied before and confirmed their expression in the TRNs, including *nkb-3*, *F36G3.2*, and *F26H9.5* (Fig. 3*E*). KEGG pathway analysis showed that the identified proteins are highly enriched in carbon metabolism, TCA cycle, oxidative phosphorylation, valine, leucine, and isoleucine degradation, and pyruvate metabolism (Fig. 3*F* and Supplemental Dataset S4). Pathway enrichment and GO analyses consistently showed that the proteins are enriched in biological processes such as the TCA cycle and other energy-producing processes (Supplemental Fig. S4, and Supplemental Dataset S4). Pathways, such as cellular structure and signaling (*e.g.*, *unc-44*/Ankyrin, *ftt-2*/14-3-3 protein), protein synthesis (*e.g.*, *rps* family ribosomal genes), membrane calcium ATPases (*e.g.*, *mca-2* and *mca-3*), and molecular chaperones (*e.g.*, *hsp-1*, *hsp-90*, *hsp-110*, *enpl-1*/HSP90B1) were also enriched (Supplemental Fig. S4 and Dataset S4).

### *Identification of Differentially Expressed Proteins Between DA and TRN Neurons*

To compare the DA and TRN proteomes obtained above, we first plotted the two sets of mass spectrometry data together. Although there was a strong correlation between the biological replicates of DA and TRN proteomes (indicating reproducibility), the correlation between DA and TRN datasets was very poor (Fig. 4*A*), suggesting that the proteomes of the two types of neurons are quite different. Clustering analysis also supports the distinct protein expression patterns between DA and TRN neurons (Fig. 4*B*).

Although the above SILAC approach allowed the identification of proteins expressed in DA and TRN neurons, the results were somewhat biased towards the more abundant proteins in the neurons. To identify proteins that are differentially expressed between two neuron types, we modified the SILAC setup to grow the strain with DA-specific expression of *Ce*MetRS L43G in “heavy” medium containing the photo-ANA probe, while growing the strain with TRN-specific expression of *Ce*MetRS L43G in “light” medium that also contains photo-ANA (Fig. 5*A*). This experimental design allows the enrichment of proteins from both DA and TRN neurons in the same experiment while identifying the proteins differentially expressed between the two types of neurons based on the H/L ratio. However, the total amount of proteins from the eight DA neurons was higher than the total amount of proteins from the six TRNs, which caused the $Log_2$(H/L) values to be skewed towards the positive numbers (Supplemental Fig. S5*A*). To address this input bias, we normalized the mass-spec results against peptide abundance, thereby centering the H/L ratios at approximately one and the $Log_2$(H/L) at around 0 (Supplemental Fig. S5*B*). This normalization approach allowed us to identify proteins with

$Log_2$(H/L) ratio and statistical significance [$-Log_{10}$($p$-adj)]. Proteins meeting both enrichment and significance thresholds [$Log_2$(H/L) > 0.5 and $-Log_{10}$($p$-adj) > 1.3] are highlighted in *red*. The corresponding pie chart (*right*) shows the mRNA expression distribution of these proteins in DA neurons. The full list can be found in Supplemental Dataset S1. *D*, the Venn diagram shows the overlap of proteins meeting the criteria from (*B*) and (*C*). The bar graph displays mRNA expression levels of selected proteins showing >2-fold enrichment in DA neurons compared to other tissues. mRNA levels (transcripts per million; TPM) were obtained from previous single-cell transcriptomic data. *E*, validation of novel DA neuron proteins. Fluorescent images reveal GFP expression in DA neurons in transgenic strains expressing *F17A9.4p::GFP*, *F52E4.5p::GFP*, and *cest-32p::GFP,* confirmed by co-localization with the *dat-1p::RFP* marker. Scale bar: 20 μm. *F*, pathway analysis. KEGG pathways were significantly enriched among the identified DA neuron proteins, as determined by DAVID.

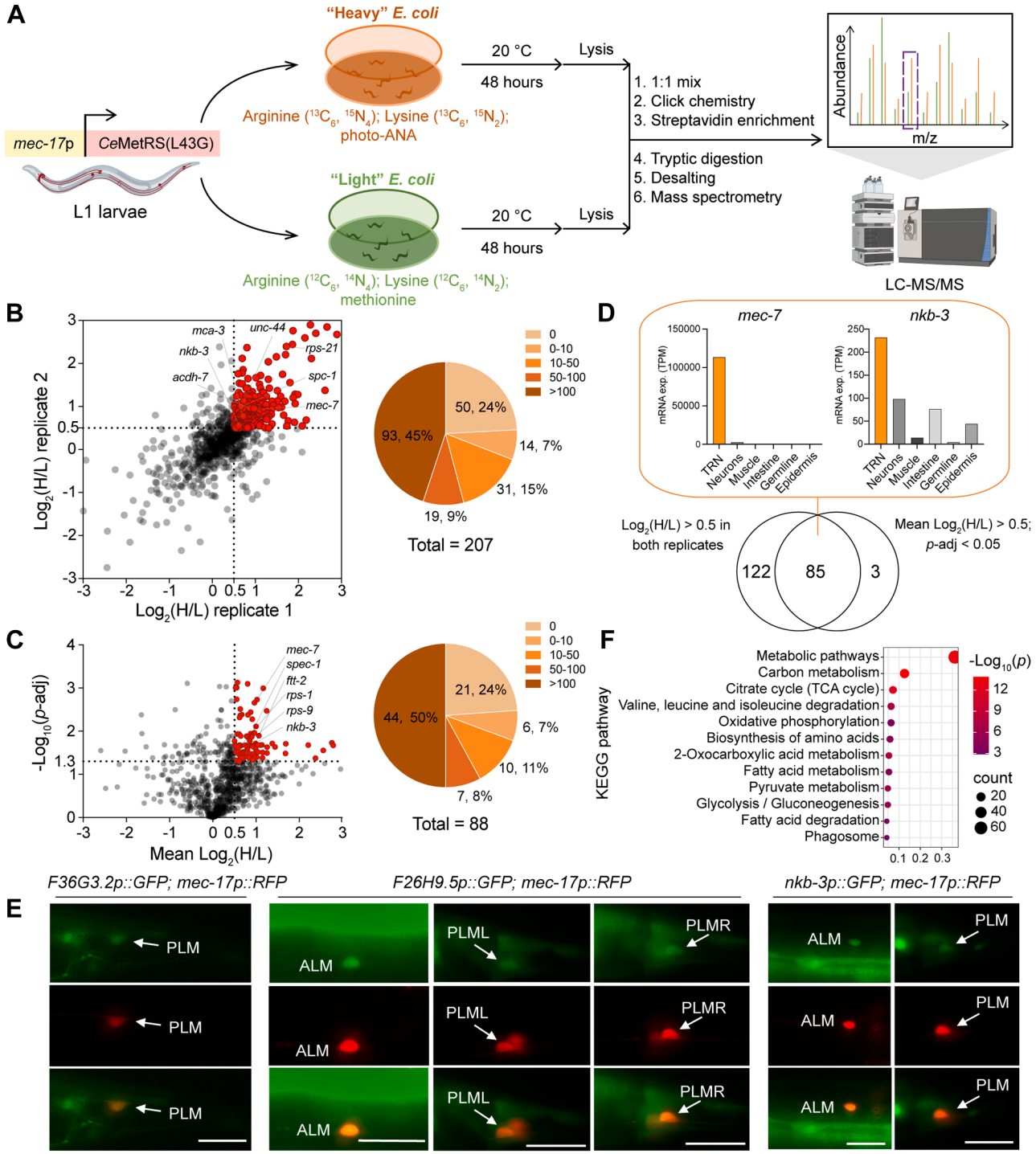


FIG. 3. **MACSPI-SILAC enables the profiling of the proteome in TRNs.** *A*, a workflow for SILAC-based protein labeling and quantification in TRNs. *B*, reproducibility of protein enrichment. Scatter plot of $Log_2$(H/L) ratios from two replicates (Pearson's correlation coefficient $r = 0.71$). Proteins consistently enriched [$Log_2$(H/L) > 0.5 in both replicates] are highlighted in *red*. The pie chart (*right*) shows the mRNA expression distribution of these proteins in TRNs. The full data can be accessed in Supplemental Dataset S3. *C*, statistical significance of protein enrichment. Volcano plot of $Log_2$(H/L) ratio versus statistical significance [$-Log_{10}$(*p*-adj)]. Proteins meeting both enrichment and significance thresholds [average $Log_2$(H/L) > 0.5 and $-Log_{10}$(*p*-adj) > 1.3] are highlighted in *red*. The pie chart shows their mRNA expression distribution in TRNs. The full data can be accessed in Supplemental Dataset S3. *D*, consensus protein set and transcriptomic validation. Venn diagram of proteins from (*B*) and (*C*). The bar graph shows high mRNA expression (TPM) in TRNs compared to other tissues for selected genes. mRNA levels (transcripts per million; TPM) were obtained from previous single-cell transcriptomic data. *E*, validation of TRN-specific protein expression. Fluorescence images show GFP expression from the promoters of *F36G3.2*, *F26H9.5*, and *nkb-3*; the GFP signal co-localizes with the RFP signal from a TRN marker *mec-17p::RFP*. Scale bar: 20 μm. *F*, functional enrichment analysis. KEGG pathways significantly enriched among the identified TRN proteins, as analyzed by DAVID.

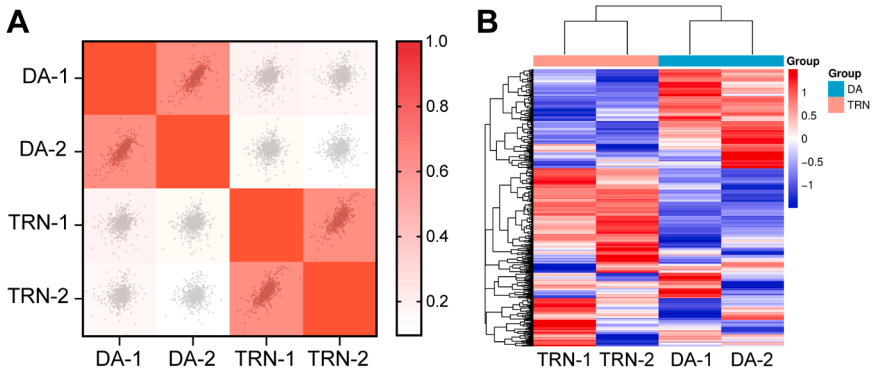


FIG. 4. **Proteomic comparisons of DA and TRN neurons in *C. elegans*.** *A*, the correlation heatmap shows the Pearson correlation coefficients between biological replicates of DA and TRN proteomes. Color intensity indicates the strength of the Pearson correlation coefficients (*red*: high correlation; *white*: low correlation). *B*, hierarchical clustering heatmap across DA and TRN proteome replicates represents similarity between samples based on protein heavy-to-light (H/L) ratio. Color intensity represents the value of $Log_2$(H/L) (*blue*: low expression; *red*: high expression).

high H/L ratios as proteins with higher expression in DA neurons and identify proteins with low H/L ratios as the ones with higher expression in TRN neurons.

When we set the threshold at $Log_2$(H/L) > 0.5 for the two replicates, we obtained 333 DA-enriched proteins (Fig. 5*B*); when we used the criteria of average $Log_2$(H/L) > 0.5 and *p*-adj <0.05, 116 DA-enriched proteins were obtained (Fig. 5*C*). Combining the two lists, we obtained a total of 336 DA-enriched proteins (Fig. 5*D*, and Supplemental Dataset S5). Applying a similar filtering method, we obtained 324 TRN-enriched proteins (Fig. 5, *B*, *C*, and *E*, and Supplemental Dataset S5). Comparing the proteomic data with single-cell transcriptomic data, we found that 73% of the DA-enriched proteins showed mRNA expression in DA neurons (enrichment fold = 2.11 and $p$ = 3.44e-50 in a hypergeometric test) and 79% of TRN-enriched proteins exhibit mRNA expression in TRNs (enrichment fold = 2.27 and $p$ = 2.83e-65 in a hypergeometric test) (Fig. 5*D* and *E*). In fact, many of the identified proteins exhibit significant mRNA expression in the respective neurons (i.e., TPM >100), suggesting that proteins with high mRNA expression levels are easier to identify than those with lower expression levels in proteomic profiling. As expected, the 336 DA-enriched proteins showed markedly higher mRNA expression in the DA neurons than in the TRNs (on average 3590.21 TPM in DA versus 1311.17 TPM in TRN) according to the scRNA-transcriptomic data. Similarly, the 324 TRN-enriched proteins showed higher mRNA expression in TRNs (4246.96 TPM on average) than in DA neurons (1051.46 TPM on average) (Dataset S5). These findings suggest that our chemoproteomic profiling approach was able to identify proteins differentially expressed between two neuron types.

KEGG pathway analysis showed that the DA-enriched proteins were significantly enriched in pathways associated with oxidative phosphorylation, carbon metabolism, lysosome, and so on (Fig. 5*F* and Supplemental Dataset S6). In contrast, TRN-enriched proteins were enriched in pathways related to motor proteins, biosynthesis of cofactors, and nucleocytoplasmic transport (Fig. 5*G* and Supplemental Dataset S6). Notably, the TRN-specific tubulin proteins MEC-12/α-tubulin and MEC-7/β-tubulin, as well as the chaperonin TCP1 complex proteins CCT-4 required for tubulin folding, were found among the proteins differentially expressed in the TRNs (59–61). On the other hand, FTT-2 (a tryptophan 5-monooxygenase activation protein involved in dopamine biosynthesis) (62) and QDPR-1 (a dihydropteridine reductase involved in monoamine synthesis) (63) were found among the proteins differentially expressed in DA neurons (Fig. 5, *B* and *C*).

Functional enrichment analysis of DA-enriched proteins revealed GO terms related to translation, protein transport, and mitochondria, whereas TRN-enriched proteins were linked to GO terms associated with TCA cycles, cytoskeletal structure, and ATP binding. These enriched pathways were generally consistent with the ones found in the two DA and TRN proteomes that were obtained in independent profiling experiments. Gene Ontology (GO) analysis further distinguished these populations: DA proteins clustered in translation, protein turnover, and mitochondrial functions (Supplemental Fig. S6 and Supplemental Dataset S6), while TRN proteins were linked to the TCA cycle, structural components, and ATP metabolism. These patterns closely matched the enrichment profiles from our independent proteomic analyses of each neuron type (Supplemental Fig. S7 and Supplemental Dataset S6).

### *Poor Correlation Between Transcriptomic and Proteomic Data for Genes in DA and TRN Neurons*

The availability of both transcriptomic and proteomic data of DA and TRN neurons allowed us to analyze the correlation of mRNA and protein levels in these neurons. To our surprise, we observed generally poor correlation between the mRNA

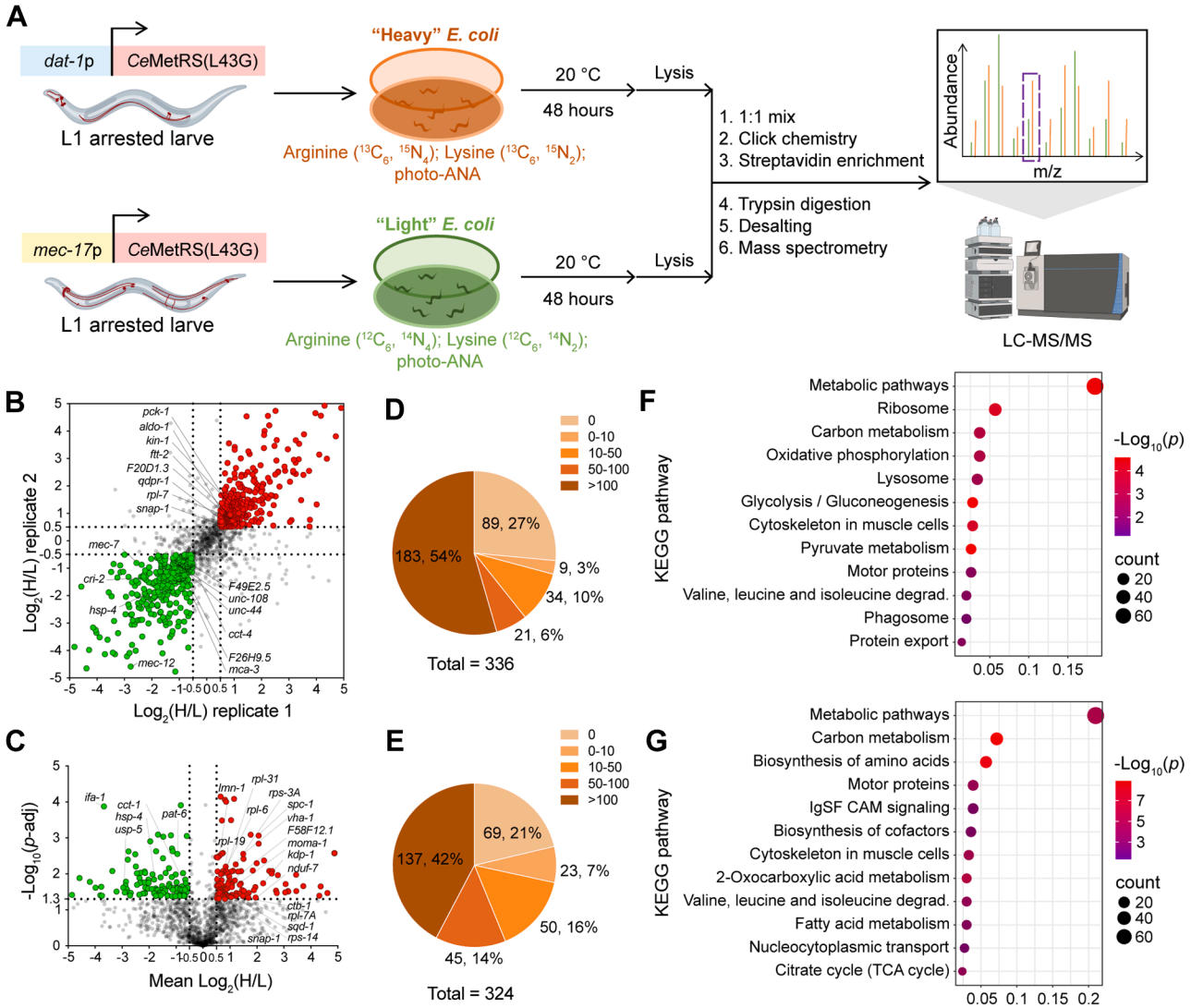


FIG. 5. **Comparative proteomic analysis of DA neurons and TRNs.** *A*, a workflow for the SILAC-based quantitative comparison of the DA and TRN proteomes. *B*, reproducibility of protein enrichment. Scatter plot of protein $Log_2$(H/L) ratios from two biological replicates (Pearson's correlation coefficient $r = 0.67$). Proteins consistently enriched in DA neurons [$Log_2$(H/L) > 0.5] or TRNs [$Log_2$(H/L) < −0.5] are highlighted in *red* and *green*, respectively. *C*, statistical significance of differential protein abundance. Volcano plot showing proteins significantly enriched in DA neurons (*red*) or TRNs (*green*), based on thresholds of $Log_2$(H/L) > 0.5 or < −0.5, respectively, and -$Log_{10}$(*p*-adj) > 1.3. *D* and *E*, neuron-specific mRNA expression. Pie charts show the mRNA expression distribution in DA neurons for proteins enriched in DA neurons (*red set*; *D*), and in TRNs for proteins enriched in TRNs (*green set*; *E*). The full protein list is in Supplemental Dataset S5. *F* and *G*, pathway enrichment. KEGG pathways are significantly enriched among proteins with high ratios (*F*, DA neuron-enriched) and low ratios (*G*, TRN-enriched), as analyzed by DAVID.

levels [$Log_2$(TPM) from single-cell transcriptomic data] and the abundance of heavy-labeled proteins [$Log_{10}$(Abundances) in proteomic profiling for individual neuron types] (Supplemental Figs. S1, *C* and *D* and S3, *B* and *C*). Pearson's correlation coefficient *r* was approximately 0.3 across all comparisons, which is consistent with previously reported correlation between mRNA and protein levels (64).

For the comparison of DA and TRN gene expression profiles, we separately compared the DA transcriptomic level with the heavy-labeled protein abundances and the TRN transcriptomic level with the light-labeled protein abundances. We observed a similarly low positive correlation between the mRNA expression levels [$Log_2$(TPM)] and corresponding protein levels [$Log_{10}$(Abundances) in the profiling of the differences between DA and TRN proteomes] (Supplemental Fig. S5, *C*–*F*). Pearson's correlation coefficient *r* was slightly above 0.3 across those comparisons. The poor concordance between transcriptomic and proteomic data indicated that mRNA levels may not be a good predictor of protein abundance in neurons, highlighting the importance of direct proteomic measurement.

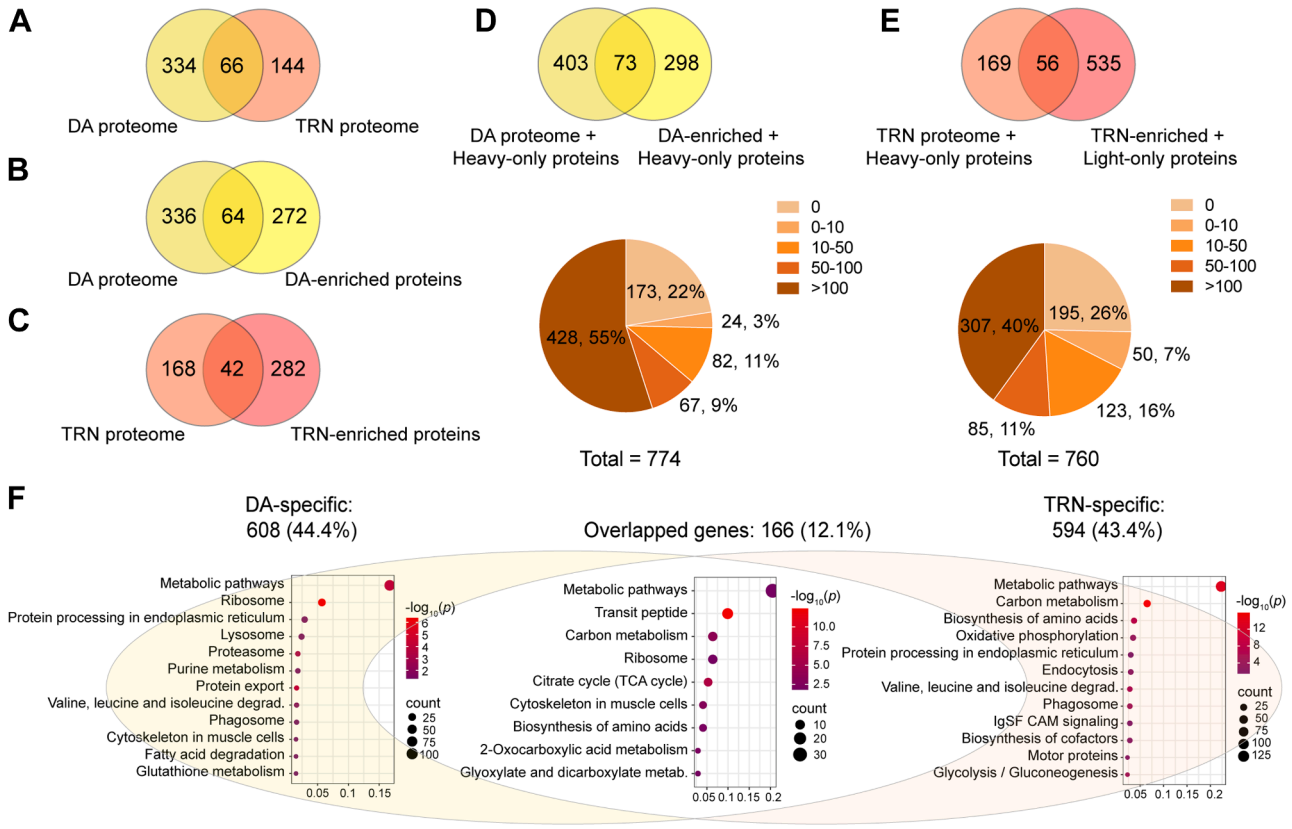


FIG. 6. **Integrated analysis of the DA and TRN neuron proteomes.** *A–C*, Venn diagrams indicate the overlap between the DA and TRN proteomes (*A*), between the DA proteome and DA-enriched proteins (*B*), and between the TRN proteome and TRN-enriched proteins (*C*). *D* and *E*, Venn diagrams show the overlaps between the expanded neuronal proteomes and the enriched proteins (*upper*). Neuron-specific mRNA expression distribution for proteins expressed in DA neurons (*D*) and TRNs (*E*). *F*, Venn diagram shows the overlap between the DA- and TRN-enriched proteins. KEGG pathways significantly enriched in the DA-specific (*left*), TRN-specific (*right*), and overlapping (*center*) protein sets. The top 10 most significant pathways for each category are displayed.

### *Comparison of DA and TRN Proteomes Using Combined Datasets*

The datasets obtained using the two different SILAC setups each have their own advantages. We observed limited overlap between the DA and TRN proteomes, suggesting divergence between the proteomes of different neuron types (Fig. 6*A*). We also observed limited overlap between DA (or TRN) proteomes and DA (or TRN)-enriched proteins (Fig. 6, *B* and *C*), indicating that the two proteomic profiling strategies likely target different groups of proteins. The DA (or TRN) versus background profiling (Figs. 2 and 3) identified proteins expressed in the DA (or TRN) neurons with likely bias towards highly abundant proteins, whereas the DA versus TRN profiling (Fig. 5) identified proteins with differential expression between the two neuron types.

To obtain a more comprehensive set of proteins for DA and TRN proteomes, we first combined the standout proteins from the two datasets (*e.g.*, combining the DA proteome in Figure 2 and DA-enriched proteins in Fig. 5). Second, we included proteins that were identified as heavy-only in both replicates or heavy-only in one replicate and $Log_2$(H/L) > 0.5 in the other replicate in the proteomic profiling experiment (from Figs. 2 and 3). Third, we also added proteins that were heavy-only in both replicates or heavy-only in one replicate and $Log_2$(H/L) > 0.5 in the other replicate in the DA vs TRN experiment to the DA proteome and added proteins that were light-only in both replicates or light-only in one replicate and $Log_2$(H/L) < −0.5 in the other replicate to the TRN proteome (from Fig. 5). The above pipeline led to a final list of 774 proteins in the DA proteome (enrichment fold = 2.23 for mRNA expression and $p$ = 4.4e-143 in a hypergeometric test; Fig. 6*D* and Supplemental Dataset S7) and 760 proteins in the TRN proteome (enrichment fold = 2.14 and $p$ = 3.5e-121 in a hypergeometric test; Fig. 6*E* and Supplemental Dataset S7).

We then used these expanded lists of proteins to analyze the differences between DA and TRN proteomes, which may provide insight into the functional specification of these neurons. Proteins identified as DA-specific are enriched in pathways associated with lysosome (important for cell homeostasis and metabolic regulation), proteosome (mediating protein degradation), and glutathione metabolism (essential

for combating dopamine-induced oxidative stress) (Fig. 6*F*). TRN-specific proteins showed significant enrichment in IgSF CAM signaling (responsible for cell adhesion and singalling), biosynthesis of cofactors (supporting enzymatic activity in energy and signaling pathways), motor proteins (essential for intracellular transport in long neuronal processes), and endocytosis (crucial for membrane recycling at mechanosensory sites). In contrast, proteins found in both DA and TRNs tend to be more enriched in basic metabolic processes (*e.g.*, TCA cycle and biosynthesis of amino acids). The abovementioned findings suggest that while DA neurons and TRNs share some core metabolic functions, their proteomes appear to be specialized to support different functions, such as neurotransmitter regulation in DA neurons and sensory transduction in TRNs, respectively.

## DISCUSSION

Our study demonstrated that MACSPI-SILAC is a robust method to label and profile neuron type-specific proteomes from intact complex tissues, bypassing the need for cell sorting while maintaining detection sensitivity for a small number of cells. In this study, we successfully profiled the proteomes of the eight dopaminergic neurons and six touch receptor neurons, representing <1% of the total number of cells (959 somatic cells and ~400 germ cells) in the animal at the L4 stage (65). Considering that neurons have significantly smaller volumes than the muscle, intestine, and epidermis cells, the amount of proteins in DA and TRN neurons is likely much lower than 1% of the total amount of proteins from the whole animal lysate. Given that most of the proteins we identified are indeed expressed in the specific neurons (evidence from single-cell RNA-seq data and independent transcriptional reporter studies), we are confident that this optimized workflow could be applied to profile the proteome of any neuron types in *C. elegans*. Expanding this approach to other cell types could eventually lead to the creation of a comprehensive, whole-organism protein atlas, which will be a valuable resource for the community.

In this study, we also demonstrated the possibility of using the MACSPI-SILAC approach to identify differentially expressed proteins between two neuron types. Traditionally, this comparison can only be done by isolating and profiling proteins from each cell type and then qualitatively comparing the proteins each type of cells expresses. This approach lacks the possibility for quantification. Alternatively, one could make a translational GFP fusion for the candidate protein and compare the GFP intensity between 2 cell types in the same animal. This approach can quantify protein levels but lacks the possibility for high-throughput analysis. By using photo-ANA to label proteins expressed in specific cells and simultaneously using “heavy” and “light” isotopes to differentiate proteins from two distinct cell types, the MACSPI-SILAC approach enabled high-throughput profiling of proteins enriched in one cell type compared to another. It can be used in conjunction with transcriptomic profiling to understand the difference in gene expression patterns between cell types.

Combining the cell-specific proteome data and single-cell transcriptomic data, we observe a generally weak correlation between mRNA and protein levels. This observation is consistent with previous reports (66, 67). We reason that the differences in detection methods may contribute to the poor correlation. For example, transcriptomic profiling involves PCR amplification, which introduces bias, whereas proteomic profiling involves the use of biased proteases like trypsin; these inherent biases may affect the accuracy of gene expression profiling. On the other hand, genuine discrepancies between the mRNA and protein levels caused by post-transcriptional regulations (*e.g.*, translational efficiency, protein stability, microRNA regulation, etc.) would also contribute to the lack of good correlation between transcriptomic and proteomic data.

The ability to profile the proteomes of specific neuron types opens new avenues in several research directions. A key application is to monitor cell-type-specific proteomic dynamics under various conditions, such as stress or disease. For instance, *C. elegans* DA neurons have been used to model the pathogenesis of Parkinson's disease (PD) through the overexpression of human α-synuclein that causes dopaminergic neurodegeneration (30). By comparing the DA proteome under physiological and pathological conditions using our method, one can identify PD-associated changes in the DA neurons at the protein levels, which may not be captured by traditional transcriptomic profiling. Similarly, one could treat the whole animal with a chemical compound and study how the pharmacological treatment alters the proteome of specific cells.

Finally, although our method uses a methionine analog for cell-specific proteome labeling, other unnatural amino acids (such as *p*-azido-L-phenylalanine and oxonorvaline) and their compatible aminoacyl-tRNA synthetase can also be used in a similar manner (68). In fact, if two amino acid probes carry different enrichment handles or identifiable tags, they may be used orthogonally in the same experiment to simultaneously profile the proteomes of 2 cell types. Moreover, although we only demonstrated the use of MACSPI-SILAC in *C. elegans*, the same principle applies to any multicellular organism. Through dietary supplementation of photo-ANA and transgenic expression of methionyl-tRNA synthetase mutants, one could, in theory, profile the proteomes of any cell types in any organisms.

### *Limitation of the Study and the Method*

One of the limitations of this study is the low number of biological replicates. Since the photo-ANA probe is a novel compound and needs to be chemically synthesized (69), studies using a large amount of the probe would be constrained by its supply. More generally, the MACSPI method has some intrinsic limitations due to the relatively low

abundance of methionine in proteins compared to other amino acids, such as leucine and serine. Even with a high incorporation rate of photo-ANA at the place of methionine during translation, the method would still be biased to identify proteins with more methionine and may have generally lower enrichment efficiency than methods using leucine and serine analogs. Moreover, the method requires transgenesis to express the MetRS mutants into the tissue-of-interest, which may be technically challenging if there are no suitable tissue-specific promoters.

## DATA AVAILABILITY

The raw mass spectrometry proteomics data have been deposited to the ProteomeXchange Consortium via the PRIDE partner repository with accession no. PXD070040 (Username: reviewer_pxd070040@ebi.ac.uk; Password: diw6GWfvAI4R). All processed data can be found in the supplementary datasets.

*Supplemental data*—This article contains supplemental data.

*Acknowledgments*—We acknowledge support by funds from the Hong Kong Research Grants Council Collaborative Research Fund (CRF C7026-20G) and General Research Fund (GRF 17106322, GRF 17105523, and GRF 17113324) to C. Z. Some strains used in this study were provided by the *Caenorhabditis* Genetics Center, which is funded by the NIH Office of Research Infrastructure Programs (P40 OD010440). Some figure panels were created with BioRender.com.

*Author contributions*—Q. R. writing–original draft; Q. R. project administration; Q. R. and S. H. methodology; Q. R. data curation; Q. R. validation; Q. R. visualization; Q. R. formal analysis; S. H. software; X. D. L. resources; C. Z. writing–review & editing; C. Z. conceptualization; C. Z. funding acquisition.

*Conflict of interest*—The authors declare the following financial interests/personal relationships which may be considered as potential competing interests: C. Z. serves as a member on the scientific advisory boards of Codexa Therapeutics, Ltd and Jorna Therapeutics, Inc.

*Abbreviations*—The abbreviations used are: BDM, 2,3-Butanedione monoxime; DA, dopaminergic neurons; GO, Gene ontology; KEGG, Kyoto Encyclopedia of Genes and Genomes; MACSPI, Methionine Analog-based Cell-Specific Proteomics and Interactomics; MetES, methionyl-tRNA synthetase; MS, mass spectrometry; PTMs, post-translational modifications; TRNs, touch receptor neurons.

Received October 31, 2025, and in revised form, February 3, 2026
Published, MCPRO Papers in Press, February 28, 2026, https://doi.org/10.1016/j.mcpro.2026.101545

## REFERENCES

1. Regev, A., Teichmann, S. A., Lander, E. S., Amit, I., Benoist, C., Birney, E., *et al*. (2017) The human cell Atlas. *eLife* **6**, e27041
2. Ahmad, R., and Budnik, B. (2023) A review of the current state of single-cell proteomics and future perspective. *Anal. Bioanal. Chem.* **415**, 6889–6899
3. Cui, M., Cheng, C., and Zhang, L. (2022) High-throughput proteomics: a methodological mini-review. *Lab. Invest.* **102**, 1170–1181
4. Budnik, B., Straubhaar, J., Neveu, J., and Shvartsman, D. (2022) In-depth analysis of proteomic and genomic fluctuations during the time course of human embryonic stem cells directed differentiation into beta cells. *Proteomics* **22**, 2100265
5. Chung, H., Parkhurst, C. N., Magee, E. M., Phillips, D., Habibi, E., Chen, F., *et al*. (2021) Joint single-cell measurements of nuclear proteins and RNA *in vivo*. *Nat. Methods* **18**, 1204–1212
6. Shim, Y.-H., and Paik, Y.-K. (2010) Caenorhabditis elegans proteomics comes of age. *PROTEOMICS* **10**, 846–857
7. Zhu, T. Y., Li, S. T., Liu, D. D., Zhang, X., Zhou, L., Zhou, R., *et al*. (2024) Single-worm quantitative proteomics reveals aging heterogeneity in isogenic Caenorhabditis elegans. *Aging Cell* **23**, e14055
8. Tan, C.-H., Wang, T.-Y., Park, H., Lomenick, B., Chou, T.-F., and Sternberg, P. W. (2024) Single-tissue proteomics in Caenorhabditis elegans reveals proteins resident in intestinal lysosome-related organelles. *Proc. Natl. Acad. Sci. U. S. A.* **121**, e2322588121
9. Masuda, M., Saimaru, H., Takamura, N., and Imai, K. (2005) An improved method for proteomics studies in C. elegans by fluorogenic derivatization, HPLC isolation, enzymatic digestion and liquid chromatography–tandem mass spectrometric identification. *Biomed. Chromatogr.* **19**, 556–560
10. Bensaddek, D., Narayan, V., Nicolas, A., Brenes Murillo, A., Gartner, A., Kenyon, C. J., *et al*. (2016) Micro-proteomics with iterative data analysis: proteome analysis in C. elegans at the single worm level. *PROTEOMICS* **16**, 381–392
11. Yuet, K. P., Doma, M. K., Ngo, J. T., Sweredoski, M. J., Graham, R. L. J., Moradian, A., *et al*. (2015) Cell-specific proteomic analysis in Caenorhabditis elegans. *Proc. Natl. Acad. Sci. U. S. A.* **112**, 2705–2710
12. Huang, S., Ran, Q., Li, X.-M., Bao, X., Zheng, C., and Li, X. D. (2024) MACSPI enables tissue-selective proteomic and interactomic analyses in multicellular organisms. *Proc. Natl. Acad. Sci. U. S. A.* **121**, e2319060121
13. Mertins, P., Udeshi, N. D., Clauser, K. R., Mani, D. R., Patel, J., Ong, S.-E., *et al*. (2012) iTRAQ labeling is superior to mTRAQ for quantitative global proteomics and phosphoproteomics. *Mol. Cell Proteomics* **11**. https://doi.org/10.1074/mcp.M111.014423
14. Marín-Vicente, C., Calvo, E., Rodríguez, J. M., Villa del Campo, C., Sierra, R., Végvári, Á., *et al*. (2024) A sample preparation procedure for isobaric labeling-based single-cell proteomics. In: Vegvari, A., Teppo, J., Zubarev, R. A., eds. *Mass Spectrometry Based Single Cell Proteomics*, Springer US, New York, NY: 33–43
15. Tsai, C.-F., Zhao, R., Williams, S. M., Moore, R. J., Schultz, K., Chrisler, W. B., *et al*. (2020) An improved boosting to amplify signal with isobaric labeling (iBASIL) strategy for precise quantitative single-cell proteomics *. *Mol. Cell Proteomics* **19**, 828–838
16. Nagarajan, A., Ning, Y., Reisner, K., Buraei, Z., Larsen, J. P., Hobert, O., *et al*. (2014) Progressive degeneration of dopaminergic neurons through TRP channel-induced cell death. *J. Neurosci.* **34**, 5738
17. Reilly, M. B., Tekieli, T., Cros, C., Aguilar, G. R., Lao, J., Toker, I. A., *et al*. (2022) Widespread employment of conserved C. elegans homeobox genes in neuronal identity specification. *PLoS Genet.* **18**, e1010372
18. Way, J. C., and Chalfie, M. (1988) mec-3, a homeobox-containing gene that specifies differentiation of the touch receptor neurons in C. elegans. *Cell* **54**, 5–16
19. Zheng, C., Jin, F. Q., Trippe, B. L., Wu, J., and Chalfie, M. (2018) Inhibition of cell fate repressors secures the differentiation of the touch receptor neurons of Caenorhabditis elegans. *Development* **145**, dev168096
20. Zhang, Y., Ma, C., Delohery, T., Nasipak, B., Foat, B. C., Bounoutas, A., *et al*. (2002) Identification of genes expressed in C. elegans touch receptor neurons. *Nature* **418**, 331–335
21. Topalidou, I., and Chalfie, M. (2011) Shared gene expression in distinct neurons expressing common selector genes. *Proc. Natl. Acad. Sci. U. S. A.* **108**, 19258–19263

22. Spencer, W. C., Zeller, G., Watson, J. D., Henz, S. R., Watkins, K. L., McWhirter, R. D., *et al*. (2011) A spatial and temporal map of C. elegans gene expression. *Genome Res.* **21**, 325–341
23. Jimeno-Martín, A., Sousa, E., Brocal-Ruiz, R., Daroqui, N., Maicas, M., and Flames, N. (2022) Joint actions of diverse transcription factor families establish neuron-type identities and promote enhancer selectivity. *Genome Res.* **32**, 459–473
24. Sulston, J., Dew, M., and Brenner, S. (1975) Dopaminergic neurons in the nematode Caenorhabditis elegans. *J. Comp. Neurol.* **163**, 215–226
25. McMillen, A., and Chew, Y. L. (2023) Neural mechanisms of dopamine function in learning and memory in Caenorhabditis elegans. *Neuronal Signal.* **8**, NS20230057
26. White, J. G., Southgate, E., Thomson, J. N., and Brenner, S. (1997) The structure of the nervous system of the nematode Caenorhabditis elegans. *Philos. Trans. R. Soc. Lond. B, Biol. Sci.* **314**, 1–340
27. Sawin, E. R., Ranganathan, R., and Horvitz, H. R. (2000) C. elegans Locomotory rate is modulated by the environment through a dopaminergic pathway and by experience through a serotonergic pathway. *Neuron* **26**, 619–631
28. Chalfie, M., Sulston, J. E., White, J. G., Southgate, E., Thomson, J. N., and Brenner, S. (1985) The neural circuit for touch sensitivity in Caenorhabditis elegans. *J. Neurosci.* **5**, 956
29. Chalfie, M., and Sulston, J. (1981) Developmental genetics of the mechanosensory neurons of Caenorhabditis elegans. *Dev. Biol.* **82**, 358–370
30. Lakso, M., Vartiainen, S., Moilanen, A.-M., Sirviö, J., Thomas, J. H., Nass, R., *et al*. (2003) Dopaminergic neuronal loss and motor deficits in Caenorhabditis elegans overexpressing human α-synuclein. *J. Neurochem.* **86**, 165–172
31. Kuwahara, T., Koyama, A., Gengyo-Ando, K., Masuda, M., Kowa, H., Tsunoda, M., *et al*. (2006) Familial parkinson mutant α-Synuclein causes dopamine neuron dysfunction in transgenic Caenorhabditis elegans. *J. Biol. Chem.* **281**, 334–340
32. Cao, S., Gelwix, C. C., Caldwell, K. A., and Caldwell, G. A. (2005) Torsin-Mediated protection from cellular stress in the dopaminergic neurons of *Caenorhabditis elegans*. *J. Neurosci.* **25**, 3801
33. Hammarlund, M., and Jin, Y. (2014) Axon regeneration in C. elegans. *Curr. Opin. Neurobiol.* **27**, 199–207
34. Chen, L., Wang, Z., Ghosh-Roy, A., Hubert, T., Yan, D., O'Rourke, S., *et al*. (2011) Axon regeneration pathways identified by systematic genetic screening in *C. elegans*. *Neuron* **71**, 1043–1057
35. Nonet, M. L., Staunton, J. E., Kilgard, M. P., Fergestad, T., Hartwieg, E., Horvitz, H. R., *et al*. (1997) *Caenorhabditis elegans rab-3* mutant synapses exhibit impaired function and are partially depleted of vesicles. *J. Neurosci.* **17**, 8061
36. Miller, K. G., Emerson, M. D., and Rand, J. B. (1999) Goα and diacylglycerol kinase negatively regulate the Gqα pathway in C. elegans. *Neuron* **24**, 323–333
37. Miller, K. G., Alfonso, A., Nguyen, M., Crowell, J. A., Johnson, C. D., and Rand, J. B. (1996) A genetic selection for Caenorhabditis elegans synaptic transmission mutants. *Proc. Natl. Acad. Sci. U. S. A.* **93**, 12593–12598
38. Kayser, E. B., Morgan, P. G., Hoppel, C. L., and Sedensky, M. M. (2001) Mitochondrial expression and function of GAS-1 in *Caenorhabditis elegans*. *J. Biol. Chem.* **276**, 20551–20558
39. Bounoutas, A., and Chalfie, M. (2007) Touch sensitivity in Caenorhabditis elegans. *Pflugers Arch.* **454**, 691–702
40. Otsuka, A. J., Franco, R., Yang, B., Shim, K. H., Tang, L. Z., Zhang, Y. Y., *et al*. (1995) An ankyrin-related gene (unc-44) is necessary for proper axonal guidance in Caenorhabditis elegans. *J. Cell Biol.* **129**, 1081–1092
41. Chen, X., and Chalfie, M. (2014) Modulation of C. elegans touch sensitivity is integrated at multiple levels. *J. Neurosci.* **34**, 6522–6536
42. Brenner, S. (1974) The genetics of Caenorhabditis elegans. *Genetics* **77**, 71–94
43. Ullrich, M., Liang, V., Chew, Y. L., Banister, S., Song, X., Zaw, T., *et al*. (2014) Bio-orthogonal labeling as a tool to visualize and identify newly synthesized proteins in Caenorhabditis elegans. *Nat. Protoc.* **9**, 2237–2255
44. Huang, D. W., Sherman, B. T., and Lempicki, R. A. (2009) Systematic and integrative analysis of large gene lists using DAVID bioinformatics resources. *Nat. Protoc.* **4**, 44–57
45. Taylor, S. R., Santpere, G., Weinreb, A., Barrett, A., Reilly, M. B., Xu, C., *et al*. (2021) Molecular topography of an entire nervous system. *Cell* **184**, 4329–4347.e4323
46. Lackner, M. R., Nurrish, S. J., and Kaplan, J. M. (1999) Facilitation of synaptic transmission by EGL-30 Gqalpha and EGL-8 PLCbeta: DAG binding to UNC-13 is required to stimulate acetylcholine release. *Neuron* **24**, 335
47. Ségalat, L., Elkes, D. A., and Kaplan, J. M. (1995) Modulation of serotonin-controlled behaviors by Go in Caenorhabditis elegans. *Science* **267**, 1648
48. Betzer, C., Lassen, L. B., Olsen, A., Kofoed, R. H., Reimer, L., Gregersen, E., *et al*. (2018) Alpha-synuclein aggregates activate calcium pump SERCA leading to calcium dysregulation. *EMBO Rep.* **19**, e44617
49. Peres, T. V., Arantes, L. P., Miah, M. R., Bornhorst, J., Schwerdtle, T., Bowman, A. B., *et al*. (2018) Role of Caenorhabditis elegans AKT-1/2 and SGK-1 in manganese toxicity. *Neurotox Res.* **34**, 584–596
50. Rose, S., Malabarba, M. G., Krag, C., Schultz, A., Tsushima, H., Di Fiore, P. P., *et al*. (2007) Caenorhabditis elegans intersectin: a synaptic protein regulating neurotransmission. *Mol. Biol. Cell* **18**, 5091–5099
51. Leroux, M. R., and Candido, E. P. M. (1997) Subunit characterization of theCaenorhabditis elegansChaperonin containing TCP-1 and expression pattern of the gene encoding CCT-1. *Biochem. Biophys. Res. Commun.* **241**, 687–692
52. Fukushige, T., Yasuda, H., and Siddiqui, S. S. (1995) Selective expression of the tba-1 α tubulin gene in a set of mechanosensory and motor neurons during the development of Caenorhabditis elegans. *Biochim. Biophys. Acta* **1261**, 401–416
53. Locke, C. J., Williams, S. N., Schwarz, E. M., Caldwell, G. A., and Caldwell, K. A. (2006) Genetic interactions among cortical malformation genes that influence susceptibility to convulsions in C. elegans. *Brain Res.* **1120**, 23–34
54. Hamelin, M., Scott, I. M., Way, J. C., and Culotti, J. G. (1992) The mec-7 beta-tubulin gene of Caenorhabditis elegans is expressed primarily in the touch receptor neurons. *EMBO J.* **11**, 2885–2893
55. Meng, L., Chen, C.-H., and Yan, D. (2016) Regulation of gap junction dynamics by UNC-44/ankyrin and UNC-33/CRMP through VAB-8 in C. elegans neurons. *PLoS Genet.* **12**, e1005948
56. Lockhead, D., Schwarz, E. M., O'Hagan, R., Bellotti, S., Krieg, M., Barr, M. M., *et al*. (2016) The tubulin repertoire of C. elegans sensory neurons and its context-dependent role in process outgrowth. *Mol. Biol. Cell* **27**, 3717–3728
57. Syntichaki, P., Samara, C., and Tavernarakis, N. (2005) The vacuolar H+ -ATPase mediates intracellular acidification required for neurodegeneration in C. elegans. *Curr. Biol.* **15**, 1249–1254
58. Chen, X., Cuadros, M. D., and Chalfie, M. (2015) Identification of nonviable genes affecting touch sensitivity in Caenorhabditis elegans using neuronally enhanced feeding RNA interference. *G3 (Bethesda)* **5**, 467–475
59. Savage, C., Xue, Y., Mitani, S., Hall, D., Zakhary, R., and Chalfie, M. (1994) Mutations in the Caenorhabditis elegans beta-tubulin gene mec-7: effects on microtubule assembly and stability and on tubulin autoregulation. *J. Cell Sci.* **107**, 2165–2175
60. Hurd, D. D. (2018) Tubulins in C. elegans. *WormBook* **2018**, 1–32
61. Lu, Y. M., and Zheng, C. (2022) The expression and function of tubulin isotypes in Caenorhabditis elegans. *Front. Cell Dev. Biol.* **10**, 860065
62. Ichimura, T., Isobe, T., Okuyama, T., Yamauchi, T., and Fujisawa, H. (1987) Brain 14-3-3 protein is an activator protein that activates tryptophan 5-monooxygenase and tyrosine 3-monooxygenase in the presence of Ca2+,calmodulin-dependent protein kinase II. *FEBS Lett.* **219**, 79–82
63. Loer, C. M., Calvo, A. C., Watschinger, K., Werner-Felmayer, G., O'Rourke, D., Stroud, D., *et al*. (2015) Cuticle integrity and biogenic amine synthesis in Caenorhabditis elegans require the cofactor tetrahydrobiopterin (BH4). *Genetics* **200**, 237–253
64. Buccitelli, C., and Selbach, M. (2020) mRNAs, proteins and the emerging principles of gene expression control. *Nat. Rev. Genet.* **21**, 630–644
65. Sulston, J. E., and Horvitz, H. R. (1977) Post-embryonic cell lineages of the nematode, Caenorhabditis elegans. *Dev. Biol.* **56**, 110–156
66. Fan, D., Cong, Y., Liu, J., Zhang, H., and Du, Z. (2024) Spatiotemporal analysis of mRNA-protein relationships enhances transcriptome-based developmental inference. *Cell Rep.* **43**, 113928
67. Wang, D., Eraslan, B., Wieland, T., Hallström, B., Hopf, T., Zolg, D. P., *et al*. (2019) A deep proteome and transcriptome abundance atlas of 29 healthy human tissues. *Mol. Syst. Biol.* **15**, e8503
68. Ngo, J. T., and Tirrell, D. A. (2011) Noncanonical amino acids in the interrogation of cellular protein synthesis. *Acc. Chem. Res.* **44**, 677–685
69. Yang, T., Li, X., and Li, X. D. (2020) A bifunctional amino acid to study protein-protein interactions. *RSC Adv.* **10**, 42076–42083